Computer Applications in Electrical Engineering
Vol. 14 *2016*
DOI 10.21008/j.1508-4248.2016.0002

Magnetic field around the screened three-phase high-current busducts

Tomasz Szczegielniak, Zygmunt Piątek, Dariusz Kusiak
Częstochowa University of Technology
42–200 Częstochowa, ul. Brzeźnicka 60a, e–mail: zygmunt.piatek@interia.pl, dariuszkusiak@wp.pl, szczegielniakt@interia.pl

This paper presents an analytical method for determining the magnetic field in the three–phase gas–insulated transmission line (*i.e.*, high-current busduct) of circular cross–section geometry. The mathematical model takes into account the skin effect and the proximity effects, as well as the complete electromagnetic coupling between phase conductors and enclosures (*i.e.*, screens). Apart from analytical calculation, computer simulations for high-current busduct system magnetic field were also performed with the aid of the commercial FEMM software, using two–dimensional finite elements.

KEYWORDS: high–current busduct, magnetic field, FEMM

1. Introduction

Today high-current busducts are applied in many projects around the world when high-power transmission of high reliability and maximum availability is required. The sizes of new projects are constantly increasing: from some hundred meters to several kilometers [1–10]. In today realizations of high–current transmission lines, we can usually see separate enclosures for each phase (Fig. 1).

Fig. 1. Three–phase high–current busduct with isolated phases [11]

High–current busducts generate extremely low frequency magnetic field, which can cause disturbances in nearby computers and some other electrical,

electronic and digital devices. Power distribution three–phase busbar systems are one of the main sources of magnetic field at industrial frequency, and can generate electromagnetic interference by inductive coupling. Moreover, the presence of a low frequency magnetic field, generated by power busbars, may produce some undesirable effect on human health [9, 10]. Thus, a correct prediction of the magnetic field generated by high current bus ducts is very important.

Magnetic field around high–current busducts depends on value of currents, but for the large cross–sectional dimensions of the phase conductor, even for industrial frequency, skin, external and internal proximity effect should be taken into account [1–7].

2. Magnetic field around three–phase high–current busduct with isolated phases

2.1. Magnetic field in the external area of the phase L_1

Let us consider the magnetic field in the screens of the flat three phase high current busduct presented in the Fig. 2.

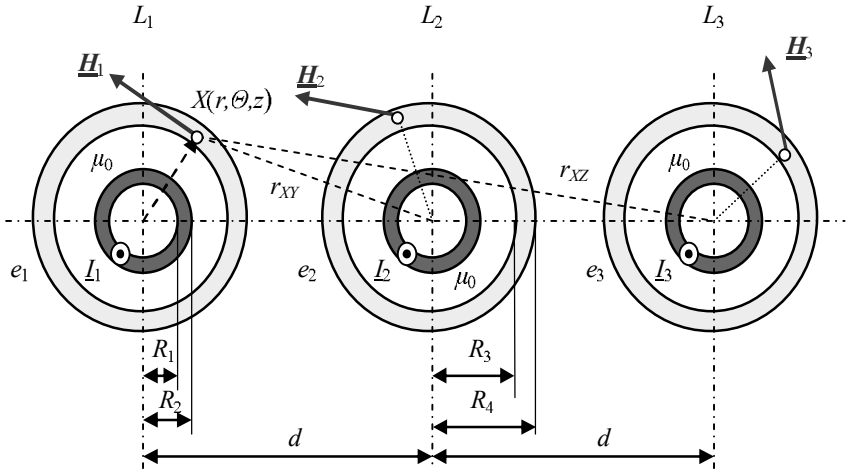

Fig. 2. High–current busduct with isolated phases

Using the Laplace's and Helmoltz's equations we can determine the magnetic field in the conductors and the screens for the three–phase high–current busducts [1–7].

The total magnetic field in the external area of the phase L_1 has a form:

$$\underline{\boldsymbol{H}}_1^{zew}(r,\Theta)=\underline{\boldsymbol{H}}_{11}^{zew}(r)+\underline{\boldsymbol{H}}_{12}^{zew}(r,\Theta)+\underline{\boldsymbol{H}}_{13}^{zew}(r,\Theta)=\mathbf{1}_r\underline{H}_{1r}^{zew}(r,\Theta)+\mathbf{1}_\Theta\underline{H}_{1\Theta}^{zew}(r,\Theta) \quad (1)$$

Magnetic field generated by current $\underline{I}_1$ is

$$\underline{\boldsymbol{H}}_{11}^{zew}(r) = \mathbf{1}_{\Theta}\underline{H}_{11\Theta}^{zew}(r) \tag{2}$$

where

$$\underline{H}_{11\Theta}^{zew}(r) = \frac{\underline{I}_1}{2\pi r} \tag{2a}$$

But magnetic field generated by $\underline{I}_2$ is defined by formula

$$\underline{\boldsymbol{H}}_{12}^{zew}(r,\Theta) = \underline{\boldsymbol{H}}_{12}^{w}(r,\Theta) + \underline{\boldsymbol{H}}_{12}^{oz}(r,\Theta) \tag{3}$$

in which magnetic field $\underline{\boldsymbol{H}}_{12}^{w}(r,\Theta)$ has two components, so

$$\underline{\boldsymbol{H}}_{12}^{w}(r,\Theta) = \mathbf{1}_r\underline{H}_{12r}^{w}(r,\Theta) + \mathbf{1}_{\Theta}\underline{H}_{12\Theta}^{w}(r,\Theta) \tag{4}$$

where radial components has a form

$$\underline{H}_{12r}^{w}(r,\Theta) = -\frac{\underline{I}_2}{2\pi r}\sum_{n=1}^{\infty}\left(\frac{r}{d}\right)^n \sin n\Theta \tag{4a}$$

and tangent component

$$\underline{H}_{12\Theta}^{w}(r,\Theta) = -\frac{\underline{I}_2}{2\pi r}\sum_{n=1}^{\infty}\left(\frac{r}{d}\right)^n \cos n\Theta \tag{4b}$$

Magnetic field $\underline{\boldsymbol{H}}_{12}^{oz}(r,\Theta)$ in the formula (3), is a so–called reverse reaction magnetic field, generated by current $\underline{I}_2$. This field has two components, radial component is:

$$\underline{H}_{12r}^{oz}(r,\Theta) = \frac{\underline{I}_2}{2\pi\,\underline{\Gamma}\,R_3\,r}\sum_{n=1}^{\infty}\left(\frac{R_4}{r}\right)^n\left(\frac{R_4}{d}\right)^n\frac{\underline{s}_{cn}}{\underline{d}_{cn}}\sin n\Theta \tag{5a}$$

and tangent component

$$\underline{H}_{\Theta}^{oz}(r,\Theta) = -\frac{\underline{I}_2}{2\pi\,\underline{\Gamma}\,R_3\,r}\sum_{n=1}^{\infty}\left(\frac{R_4}{r}\right)^n\left(\frac{R_4}{d}\right)^n\frac{\underline{s}_{cn}}{\underline{d}_{cn}}\cos n\Theta \tag{5b}$$

where

$$\underline{d}_{cn} = I_{n-1}(\underline{\Gamma}R_4)\,K_{n+1}(\underline{\Gamma}R_3) - I_{n+1}(\underline{\Gamma}R_3)\,K_{n-1}(\underline{\Gamma}R_4) \tag{5c}$$

and

$$\begin{aligned}\underline{s}_{cn} = {} & -n\frac{R_3}{R_4}K_n(\underline{\Gamma}R_4)\left[I_{n-1}(\underline{\Gamma}R_3) + I_{n+1}(\underline{\Gamma}R_3)\right] + \\ & + n\left\{2\,I_{n+1}(\underline{\Gamma}R_4)\,K_n(\underline{\Gamma}R_3) + I_n(\underline{\Gamma}R_3)\left[K_{n-1}(\underline{\Gamma}R_4) + K_{n+1}(\underline{\Gamma}R_4)\right]\right\} + \\ & + \underline{\Gamma}\,R_3\left[I_{n+1}(\underline{\Gamma}R_4)\,K_{n-1}(\underline{\Gamma}R_3) - I_{n-1}(\underline{\Gamma}R_3)\,K_{n-1}(\underline{\Gamma}R_4)\right]\end{aligned} \tag{5d}$$

In the above formulas $K_n(\underline{\Gamma}r)$, $I_{n-1}(\underline{\Gamma}r)$, $K_{n-1}(\underline{\Gamma}r)$, $I_{n+1}(\underline{\Gamma}r)$ and $K_{n+1}(\underline{\Gamma}r)$ are modified Bessel's functions, n, n–1 and n+1 order, calculated for $r = R_3$ and $r = R_4$, and the complex propagation constant of electromagnetic wave in the conductive material equals

$$\underline{\Gamma} = \sqrt{\mathrm{j}\omega\mu\gamma} = \sqrt{\omega\mu\gamma}\,\exp[\mathrm{j}\frac{\pi}{4}] = k + \mathrm{j}\,k = \sqrt{2\mathrm{j}}\,k \tag{6}$$

and the attenuation constant

$$k = \sqrt{\frac{\omega\mu\gamma}{2}} = \frac{1}{\delta} \tag{7}$$

where δ is the electrical skin depth of the electromagnetic wave penetration into the conducting environment, ω is an angular frequency, γ means conductivity of the material, and $\mu_0 = 4\pi\,10^{-7}\ \mathrm{H\cdot m^{-1}}$ is magnetic permeability of the vacuum.

Finally, the magnetic field of the phase L_1, generated by current $\underline{I}_2$ has a form

$$\underline{\boldsymbol{H}}_{12}^{zew}(r,\Theta) = \mathbf{1}_r\,\underline{H}_{12r}^{zew}(r,\Theta) + \mathbf{1}_\Theta\,\underline{H}_{12\Theta}^{zew}(r,\Theta) \tag{8}$$

where components take the following forms

$$\underline{H}_{12r}^{zew}(r,\Theta) = -\frac{\underline{I}_2}{2\pi r}\sum_{n=1}^{\infty}\left[\left(\frac{r}{d}\right)^n - \frac{1}{\underline{I}'R_3}\left(\frac{R_4}{r}\right)^n\left(\frac{R_4}{d}\right)^n\frac{\underline{s}_{cn}}{\underline{d}_{cn}}\right]\sin n\Theta \tag{8a}$$

and

$$\underline{H}_{12\Theta}^{zew}(r,\Theta) = -\frac{\underline{I}_2}{2\pi r}\sum_{n=1}^{\infty}\left[\left(\frac{r}{d}\right)^n + \frac{1}{\underline{I}'R_3}\left(\frac{R_4}{r}\right)^n\left(\frac{R_4}{d}\right)^n\frac{\underline{s}_{cn}}{\underline{d}_{cn}}\right]\cos n\Theta \tag{8b}$$

In the same way can be determined the magnetic field generated by current $\underline{I}_3$. This field has a form

$$\underline{\boldsymbol{H}}_{13}^{zew}(r,\Theta) = \mathbf{1}_r\,\underline{H}_{13r}^{zew}(r,\Theta) + \mathbf{1}_\Theta\,\underline{H}_{13\Theta}^{zew}(r,\Theta) \tag{9}$$

in which the radial component is

$$\underline{H}_{13r}^{zew}(r,\Theta) = -\frac{\underline{I}_3}{2\pi r}\sum_{n=1}^{\infty}\left[\left(\frac{r}{2d}\right)^n - \frac{1}{\underline{I}'R_3}\left(\frac{R_4}{r}\right)^n\left(\frac{R_4}{2d}\right)^n\frac{\underline{s}_{cn}}{\underline{d}_{cn}}\right]\sin n\Theta \tag{9a}$$

and the tangent component is

$$\underline{H}_{13\Theta}^{zew}(r,\Theta) = -\frac{\underline{I}_3}{2\pi r}\sum_{n=1}^{\infty}\left[\left(\frac{r}{2d}\right)^n + \frac{1}{\underline{I}'R_3}\left(\frac{R_4}{r}\right)^n\left(\frac{R_4}{2d}\right)^n\frac{\underline{s}_{cn}}{\underline{d}_{cn}}\right]\cos n\Theta \tag{9b}$$

2.2. Magnetic field in the external area of the phase L_2

The total magnetic field in the external area of the phase L_2 has a form:

$$\underline{\boldsymbol{H}}_2^{zew}(r,\Theta) = \underline{\boldsymbol{H}}_{22}^{zew}(r) + \underline{\boldsymbol{H}}_{21}^{zew}(r,\Theta) + \underline{\boldsymbol{H}}_{23}^{zew}(r,\Theta) = \mathbf{1}_r\,\underline{H}_{2r}^{zew}(r,\Theta) + \mathbf{1}_\Theta\,\underline{H}_{2\Theta}^{zew}(r,\Theta) \tag{10}$$

The magnetic field generated by current $\underline{I}_2$ is

$$\underline{\boldsymbol{H}}_{22}^{zew}(r) = \mathbf{1}_\Theta\,\underline{H}_{22\Theta}^{zew}(r) \tag{11}$$

where

$$\underline{H}_{22\Theta}^{zew}(r)=\frac{\underline{I}_2}{2\pi r} \tag{11a}$$

Magnetic field generated by current $\underline{I}_1$ has a form

$$\underline{\boldsymbol{H}}_{21}^{zew}(r,\Theta)=\mathbf{1}_r\underline{H}_{21r}^{zew}(r,\Theta)+\mathbf{1}_\Theta\underline{H}_{21\Theta}^{zew}(r,\Theta) \tag{12}$$

where components take the following forms

$$\underline{H}_{21r}^{zew}(r,\Theta)=-\frac{\underline{I}_1}{2\pi r}\sum_{n=1}^{\infty}(-1)^n\left[\left(\frac{r}{d}\right)^n-\frac{1}{\underline{\Gamma}'R_3}\left(\frac{R_4}{r}\right)^n\left(\frac{R_4}{d}\right)^n\frac{\underline{s}_{cn}}{\underline{d}_{cn}}\right]\sin n\Theta \tag{12a}$$

and

$$\underline{H}_{21\Theta}^{zew}(r,\Theta)=-\frac{\underline{I}_1}{2\pi r}\sum_{n=1}^{\infty}(-1)^n\left[\left(\frac{r}{d}\right)^n+\frac{1}{\underline{\Gamma}R_3}\left(\frac{R_4}{r}\right)^n\left(\frac{R_4}{d}\right)^n\frac{\underline{s}_{cn}}{\underline{d}_{cn}}\right]\cos n\Theta \tag{12b}$$

Whereas the magnetic field generated by current $\underline{I}_3$ is defined by formula

$$\underline{\boldsymbol{H}}_{23}^{zew}(r,\Theta)=\mathbf{1}_r\underline{H}_{23r}^{zew}(r,\Theta)+\mathbf{1}_\Theta\underline{H}_{23\Theta}^{zew}(r,\Theta) \tag{13}$$

in which the radial component takes the following form

$$\underline{H}_{23r}^{zew}(r,\Theta)=-\frac{\underline{I}_3}{2\pi r}\sum_{n=1}^{\infty}\left[\left(\frac{r}{d}\right)^n-\frac{1}{\underline{\Gamma}'R_3}\left(\frac{R_4}{r}\right)^n\left(\frac{R_4}{d}\right)^n\frac{\underline{s}_{cn}}{\underline{d}_{cn}}\right]\sin n\Theta \tag{13a}$$

while the tangent component is

$$\underline{H}_{23\Theta}^{zew}(r,\Theta)=-\frac{\underline{I}_3}{2\pi r}\sum_{n=1}^{\infty}\left[\left(\frac{r}{d}\right)^n+\frac{1}{\underline{\Gamma}R_3}\left(\frac{R_4}{r}\right)^n\left(\frac{R_4}{d}\right)^n\frac{\underline{s}_{cn}}{\underline{d}_{cn}}\right]\cos n\Theta \tag{13b}$$

2.3. Magnetic field in the external area of the phase L_3

The total magnetic field in the external area of the phase L_3 has a form:

$$\underline{\boldsymbol{H}}_3^{zew}(r,\Theta)=\underline{\boldsymbol{H}}_{33}^{zew}(r)+\underline{\boldsymbol{H}}_{32}^{zew}(r,\Theta)+\underline{\boldsymbol{H}}_{31}^{zew}(r,\Theta)=\mathbf{1}_r\underline{H}_{3r}^{zew}(r,\Theta)+\mathbf{1}_\Theta\underline{H}_{3\Theta}^{zew}(r,\Theta) \tag{14}$$

Magnetic field generated by current $\underline{I}_3$ is

$$\underline{\boldsymbol{H}}_{33}^{zew}(r)=\mathbf{1}_\Theta\underline{H}_{33\Theta}^{zew}(r) \tag{15}$$

where

$$\underline{H}_{11\Theta}^{zew}(r)=\frac{\underline{I}_3}{2\pi r} \tag{15a}$$

Magnetic field generated by current $\underline{I}_2$ has a form

$$\underline{\boldsymbol{H}}_{32}^{zew}(r,\Theta)=\mathbf{1}_r\underline{H}_{32r}^{zew}(r,\Theta)+\mathbf{1}_\Theta\underline{H}_{32\Theta}^{zew}(r,\Theta) \tag{16}$$

where components take the following forms

$$\underline{H}_{32r}^{zew}(r,\Theta) = -\frac{\underline{I}_2}{2\pi r}\sum_{n-1}^{\infty}(-1)^n\left[\left(\frac{r}{d}\right)^n - \frac{1}{\underline{\Gamma}R_3}\left(\frac{R_4}{r}\right)^n\left(\frac{R_4}{d}\right)^n\frac{\underline{s}_{cn}}{\underline{d}_{cn}}\right]\sin n\Theta \quad (17a)$$

and

$$\underline{H}_{32\Theta}^{zew}(r,\Theta) = -\frac{\underline{I}_2}{2\pi r}\sum_{n=1}^{\infty}(-1)^n\left[\left(\frac{r}{d}\right)^n + \frac{1}{\underline{\Gamma}R_3}\left(\frac{R_4}{r}\right)^n\left(\frac{R_4}{d}\right)^n\frac{\underline{s}_{cn}}{\underline{d}_{cn}}\right]\cos n\Theta \quad (17b)$$

Whereas the magnetic field generated by current $\underline{I}_1$ is defined by formula

$$\underline{\boldsymbol{H}}_{31}^{zew}(r,\Theta) = \mathbf{1}_r\,\underline{H}_{31r}^{zew}(r,\Theta) + \mathbf{1}_\Theta\,\underline{H}_{31\Theta}^{zew}(r,\Theta) \quad (18)$$

in which the radial component takes the following form

$$\underline{H}_{31r}^{zew}(r,\Theta) = -\frac{\underline{I}_1}{2\pi r}\sum_{n=1}^{\infty}(-1)^n\left[\left(\frac{r}{2d}\right)^n - \frac{1}{\underline{\Gamma}R_3}\left(\frac{R_4}{r}\right)^n\left(\frac{R_4}{2d}\right)^n\frac{\underline{s}_{cn}}{\underline{d}_{cn}}\right]\sin n\Theta \quad (18a)$$

while the tangent component

$$\underline{H}_{131\Theta}^{zew}(r,\Theta) = -\frac{\underline{I}_1}{2\pi r}\sum_{n-1}^{\infty}(-1)^n\left[\left(\frac{r}{2d}\right)^n + \frac{1}{\underline{\Gamma}R_3}\left(\frac{R_4}{r}\right)^n\left(\frac{R_4}{2d}\right)^n\frac{\underline{s}_{cn}}{\underline{d}_{cn}}\right]\cos n\Theta \quad (18b)$$

3. Numerical example

Based on the derived formulae, the magnetic field in the high–current busduct depicted in figure 2 were calculated. Calculations were made for high–current busduct produced by Electrobudowa SA (for model ELPE–36/15 [13]). According to the notation applied in figure 2, the following geometry of the busduct has been selected: $R_1 = 0.236$ m, $R_2 = 0.25$ m, $R_3 = 0.594$ m, $R_4 = 0.6$ m, $d = 1.8$ m. Both the phase conductors and the screens are made of aluminium, which has an electric conductivity of $\gamma = 35$ MS·m^{-1}. The frequency is 50 Hz. Currents in the phase conductors are

$$\underline{I}_1 = 15000\exp[-\mathrm{j}\,0]\,\mathrm{A},\quad \underline{I}_2 = 15000\exp[-\mathrm{j}\frac{2}{3}\pi]\,\mathrm{A},\quad \underline{I}_3 = 15000\exp[\mathrm{j}\frac{2}{3}\pi]\,\mathrm{A}.$$

The results of the analytical calculations of the magnetic field around the ELPE high–current busduct are presented in the Figure 3.

Apart from analytical calculation, computer simulations for high–current busduct the magnetic field were also performed with the aid of the commercial FEMM software [12]. The magnetic field distribution around ELPE high–current busduct is presented in the Figure 4.

For comparative purposes, the magnetic field along the sections A, B, C, D, presented in the Figure 5, was calculated.

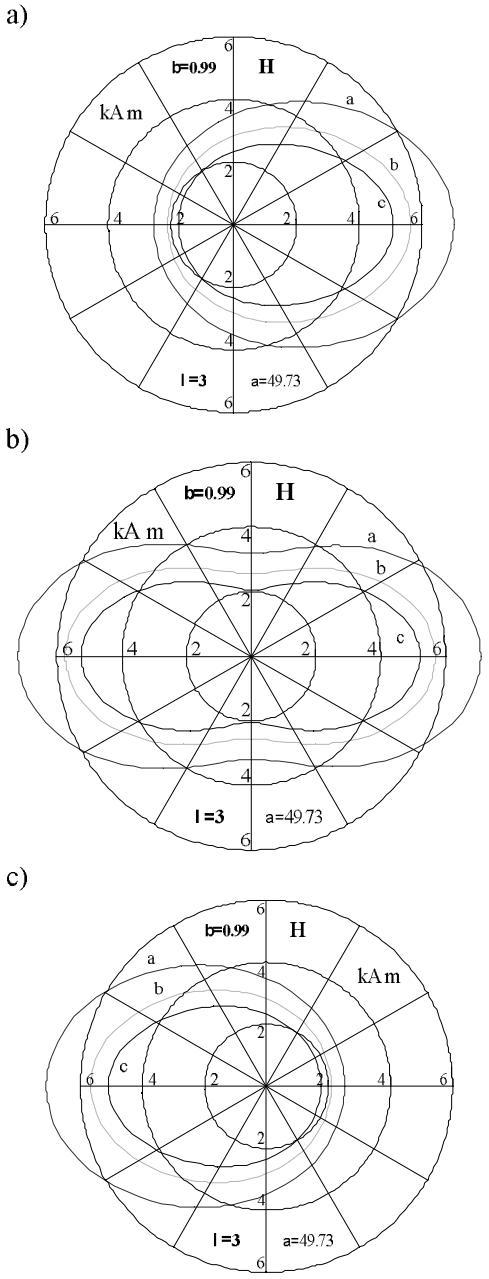

Fig. 3. Magnetic field distribution for ELPE high current busduct (red line: $r = R_4$, green line: $r - R_4 + 0.15$, blue line: $r - R_4 + 0.3$, $\beta = \frac{R_1}{R_2}$, $\lambda = \frac{d}{R_2}$, $\alpha = \frac{R_2}{\delta} = k\,R_2$):
a) phase L_1; b) phase L_2; c) phase L_3

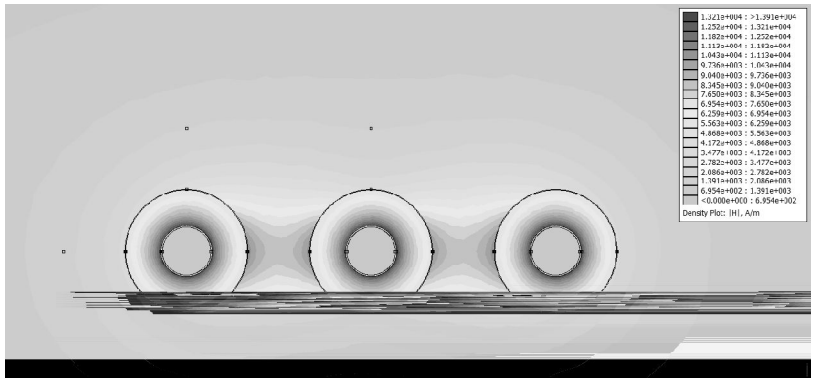

Fig. 4. Magnetic field distribution around ELPE high current busduct

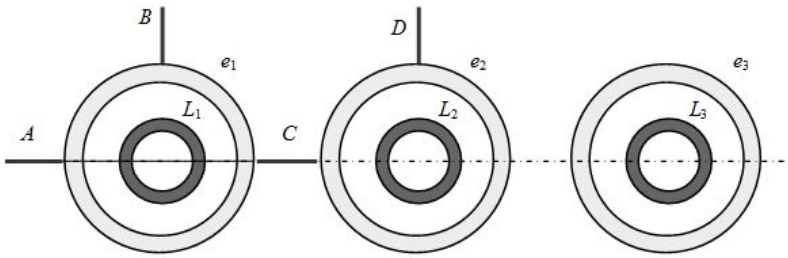

Fig. 5. ELPE high–current busduct with marked sections A, B, C, D

In the Figure 6 presented is the magnetic field distribution along sections A, B, C, D.

a)

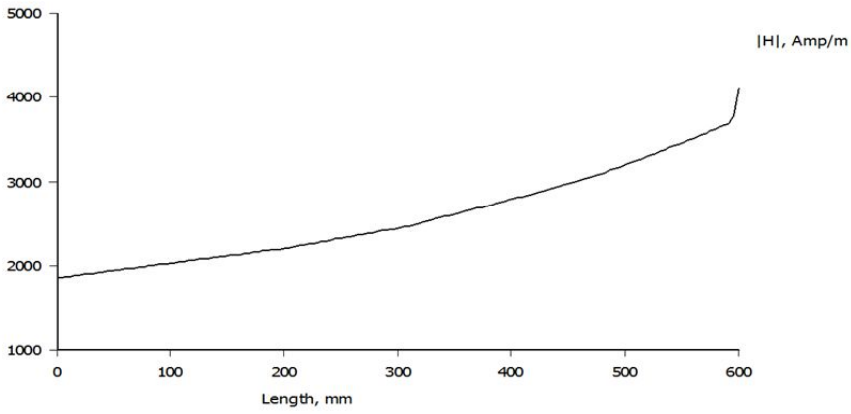

Fig. 6. Magnetic field distribution along sections a) A, b) B, c) C, d) D

b)

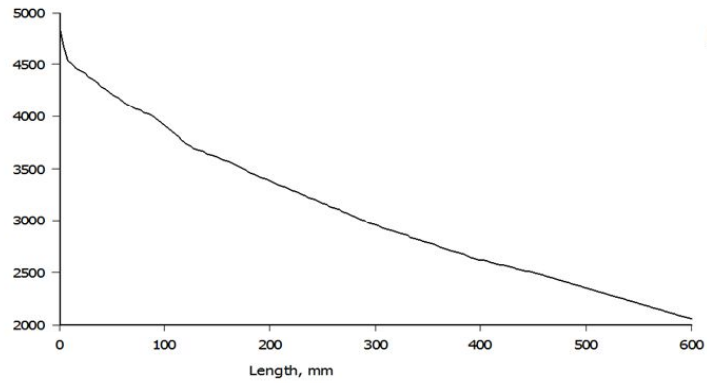

c)

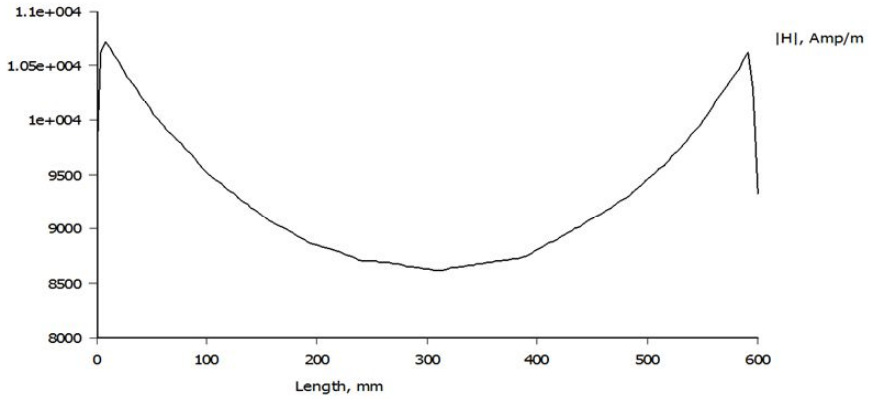

d)

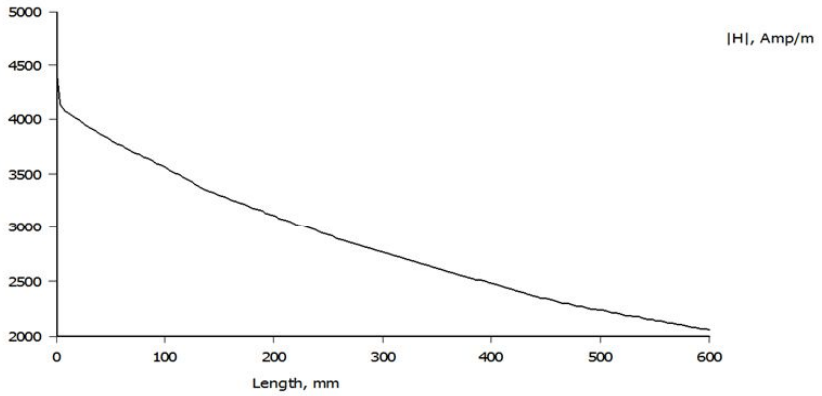

Fig. 6 cont. Magnetic field distribution along sections a) A, b) B, c) C, d) D

4. Conclusions

The paper presents an analytical method for determining the magnetic field in the three–phase high–current busduct of circular cross–section geometry. The mathematical model takes into account the skin effect and the proximity effects. To verify the analytical formulae authors performed computations by means of the finite element method.

The magnetic field around the high–current busducts are usually calculated numerically with the use of a computer. However, the analytical calculation of the electromagnetic field is preferable, because it results in a mathematical expression for showing its dependences on various parameters of the line arrangement.

From Figure 3 and 6 results that the magnetic field calculated on the basis analytical formulae is lower than the magnetic field determined by FEMM software. These differences could be caused that the phase conductors in the analytical method are treated as the filnaments.

References

[1] Nawrowski R.: Tory wielkoprądowe izolowane powietrzem lub SF_6. Wyd. Pol. Poznańskiej, Poznań 1998.

[2] Piątek Z.: Impedances of high–current busducts. Wyd. P. Częstochowskiej, Częstochowa 2008.

[3] Piątek Z.: Pole magnetyczne w otoczeniu jednobiegunowych osłoniętych torów wielkoprądowych. Zesz. Nauk. P. Śląskiej 1999, Elektryka, z. 166.

[4] Piątek Z., Kusiak D., Szczegielniak T.: Pole magnetyczne oddziaływania zwrotnego w dwuprzewodowym nieekranowanym torze wielkoprądowym, XV Conference Computer Applications in Electrical Engineering, Poznań 2010, ss. 33–34.

[5] Kusiak D., Piątek Z., Szczegielniak T.: The Asymmetry of the Magnetic Field Distribution in a Flat Unshielded 3–Phase High Current Busduct, Acta Technica Jaurinensis Vol.6 nr 1, s.49–55, 2013.

[6] Piatek, Z.: Method of Calculating Total Eddy Currents Induced in Screens of a Symmetrical Three–Phase Single–Pole Gas–Insulated Transmission Line, Acta Technica CSAV 53, 2008, pp. 103–120.

[7] Piątek Z.: Modelowanie linii, kabli i torów wielkoprądowych. Wyd. P. Częstochowskiej, Częstochowa 2007.

[8] Koch, H.: Gas–Insulated Transmission Lines (GIL). John Wiley & Sons, 2012.

[9] CIGRE TB 218.: Gas Insulated Transmission Lines (GIL, CIGRE, Paris, France, 2003.

[10] CIGRE TB 351.: Application of Long High Capacity Gas Insulated Lines (GIL), CIGRE, Paris, France, 2008.

[11] Holduct – Z. H. Ltd. Polska.: Szynoprzewody trójfazowe okrągłe. [Online]. Available: http://www.holduct.com.pl/index.php?menu=p2

[12] Meeker, D.C., Finite Element Method Magnetics, version 4.2 (11apr2012, Mathematica Build), http://www.femm.info.
[13] Elektrobudowa SA Katowice: Jednofazowe przewody ekranowane ELPE, [Online] Available: http://www.busduct.pl/main/produkty_busduct/idp:121.html

(Received: 29. 09. 2016, revised: 16. 11. 2016)